frontiers in Materials

ORIGINAL RESEARCH
published: 02 March 2022
doi: 10.3389/fmats.2022.843522

Imidazo [1,2-a] Pyrimidine Derivatives as Effective Inhibitor of Mild Steel Corrosion in HCl Solution: Experimental and Theoretical Studies

*Kun Cao, Wenheng Huang, Xi Huang and Jie Pan**

School of Chemistry and Chemical Engineering, Neijiang Normal University, Neijaing, China

The inhibitory performance of imidazole [1,2-a] pyrimidine derivatives, namely, 2,4-diphenylbenzo [4,5]imidazo [1,2-a]pyrimidine (DPIP) and 2-(4-octylphenyl)-4-phenylbenzo [4,5]imidazo [1,2-a]pyrimidine (OPIP), against mild steel corrosion in 1 mol L^{-1} HCl solution was studied by weight loss at different temperatures, potentiodynamic polarization curves (PDP), electrochemical impedance spectroscopy (EIS), and surface analysis technology. The two corrosion inhibitors showed an outstanding inhibition performance, and the inhibition efficiency achieved 91.9% for OPIP and 90.5% for DPIP at a concentration of 0.1 mmol L^{-1}. Electrochemical methods showed that DPIP and OPIP behaved as mixed-type inhibitors. Density function theory (DFT) and molecular dynamic simulation (MD) were approached to theoretically study the relationship of the inhibitor structure and anti-corrosion performance, which were also compatible with the weight loss and electrochemical observations.

Keywords: corrosion, imidazo pyrimidine, inhibitor, EIS, dynamic simulation

OPEN ACCESS

Edited by:
Binbin Zhang,
Institute of Oceanology (CAS), China

Reviewed by:
Yujie Qiang,
University of Science and Technology Beijing, China
Lei Guo,
Tongren University, China

****Correspondence:***
Jie Pan
figock01@163.com

Specialty section:
This article was submitted to Environmental Degradation of Materials, a section of the journal Frontiers in Materials

Received: *26 December 2021*
Accepted: *20 January 2022*
Published: *02 March 2022*

Citation:
Cao K, Huang W, Huang X and Pan J (2022) Imidazo [1,2-a] Pyrimidine Derivatives as Effective Inhibitor of Mild Steel Corrosion in HCl Solution: Experimental and Theoretical Studies. Front. Mater. 9:843522. doi: 10.3389/fmats.2022.843522

1 INTRODUCTION

Mild steel is widely used in transportation, construction, medical equipment, and other fields, which has an extremely important impact on human life and social production. Unfortunately, Q235 steel is susceptible to corrosion in harsh work environments, and it is prone to breakage after being corroded, which not only causes enormous economic losses but also threatens people's lives. Hence, the corrosion protection of metal materials is particularly important. A corrosion inhibitor is one of the best ways to inhibit metal corrosion in a harsh corrosive environment such as salt solution or acid solution through surface adsorption. Due to the moderate price of these products, this method is easy to carry out and cheap. A large number of studies conducted in the past 50 years have produced inorganic, organic, or plant extract products suitable for specific corrosion systems (metal/corrosive media) (Li et al., 2021). The organic corrosion inhibitor needs at least polar groups, through which molecules can combine the metal surface, such as the functional group(s) with a heteroatom(s) (N, P, O, or S) containing lone pair electrons; the combination between the molecule and the metal surface can also achieved through the interaction between the delocalized "π" electron of the double bond or aromatic ring and the "d" orbital of the metal. In addition, the shape or size of the corrosion inhibitor molecule has a great impact on its performance (El Azzouzi et al., 2016; Zarrouk et al., 2016; Salim et al., 2019; Meeusen et al., 2020; Mishra et al., 2020). As seen previously, heterocyclic compounds have been studied by many researchers such as benzimidazoles, quinoxaline, oxazole, imidazole,

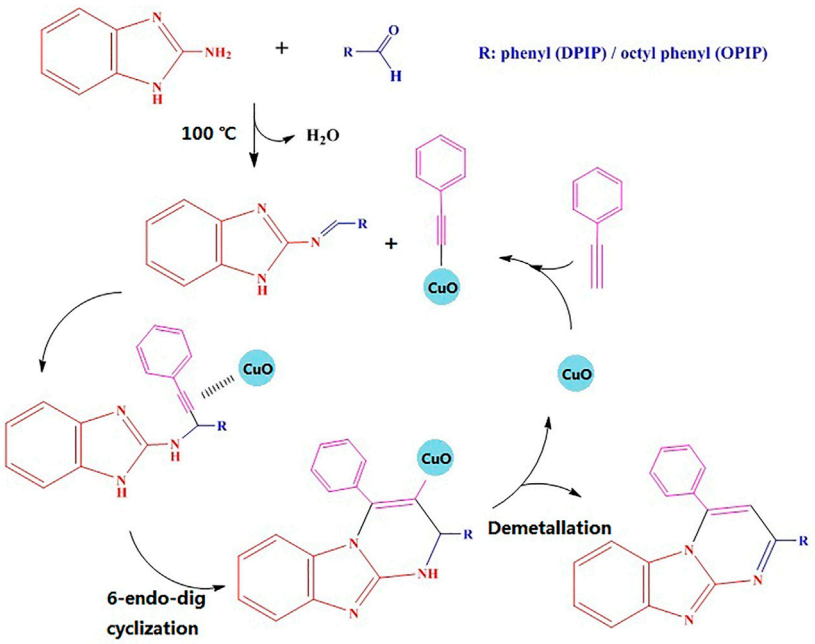

FIGURE 1 | Mechanism for synthesis of imidazo [1,2-a] pyrimidine compounds.

quinoline, and tetrazole (Zhang et al., 2019a; Zhang et al., 2019b; El-Hajjaji et al., 2019; Qiang et al., 2020; Qiang et al., 2021). In addition, with the increase in the number of unsaturated bonds in the molecules, the corrosion inhibition performance of these compounds is improved. Imidazole pyrimidine and its derivatives are commonly used as antibacterial, antiviral, anti-inflammatory, and antitumor drugs. It has heterocyclic groups such as imidazole and pyrimidine and is a potential corrosion inhibitor to protect steel from environmental corrosion (Anejjar et al., 2015; Ech-chihbi et al., 2017).

In this work, we mainly aimed to investigate the two imidazole pyrimidine derivatives as potential corrosion inhibitors for mild steel in an acidic environment and the corrosion inhibition mechanism. Understanding of the mechanism can allow for the most profitable use of these corrosion inhibitors and the optimization of more effective compounds. Therefore, the anti-corrosion properties of the inhibitors were investigated by weight loss, electrochemical methods, and the characterization of the metal surface treated by scanning electron microscopy (SEM), atomic force microscopy (AFM), and X-ray photoelectron spectroscopy (XPS). A correlation between inhibitory activity and molecular structures was investigated using the density functional theory (DFT) method and dynamic molecular simulation.

2 EXPERIMENTAL

2.1 Chemical Synthesis of Organic Compounds

The route for the synthesis of the two imidazo pyrimidine compounds is shown in **Figure 1**. Briefly, 0.5 mmol 2-aminobenzimidazole, 0.5 mmol benzaldehyde (or 4-Octylbenzaldehyde), 0.5 mmol phenylacetylene, and 10 mg copper oxide nanoparticles were stirred at 100°C under solvent-free condition until the consumption of 2-aminobenzimidazole. After completion of the reaction, ethanol was added to the reaction mixture, and then the catalyst was separated by centrifugation. The organic layer was concentrated under rotary evaporation to afford the crude product, which was purified by column chromatography. For 2,4-diphenylbenzo [4,5] imidazo [1,2-a]pyrimidine (DPIP), ^{1}H NMR (CDCl3, 400 MHz) δ 8.24 (br, 2H), 7.91 (d, 1H), 7.66–7.37 (m, 9H), 7.19 (s, 1H), 6.96 (t, 1H, J = 8.24 Hz), 6.62 (d, 1H, J = 8.4 Hz); For 2-(4-octylphenyl)-4-phenylbenzo [4,5]imidazo [1,2-a]pyrimidine (OPIP), ^{1}H NMR (CDCl3, 400 MHz) δ 8.23 (d, J = 8.24 Hz, 2H), 7.95–7.97 (m, 1H), 7.63–7.72 (m, 5H), 7.44 (t, J = 7.33 Hz, t), 7.34 (d, J = 8.24 Hz, 2H), 7.24 (s, 1H), 7.01 (t, J = 8.01 Hz, 1H), 6.66–6.68 (m, 1H), 2.69 (t, J = 7.79 Hz, 2H), 1.26–1.69 (m, 12H), 0.91 (t, J = 7.33 Hz, 3H);

2.2 Material and Solution Preparation

The mild steel samples used in this study have a chemical composition (% by weight) Fe = 99.13, S = 0.07, P = 0.10, Si = 0.39, Al = 0.02, Mn = 0.07, and C = 0.22. All mild steel samples in this work were polished using 200–2000 grand SiC paper and 0.5 μm Al_2O_3 powder, washed with distilled water, degreased with acetone, and dried in the cool air. HCl solution (1 mol L^{-1}) is obtained by dilution of 37% hydrochloride acid using distilled water. Inhibitor stock solution (1 mmol/L) was prepared by dissolving DPIP and OPIP in a 30% by volume of ethyl alcohol in 1 mol L^{-1} HCl solution, and the required concentration of inhibitors were prepared by dilution using 1 mol L^{-1} HCl

solution. The amount of ethyl alcohol in all aqueous solution in the presence and the absence of the investigated nutmeg oil were kept constant to remove the effect of the ethyl alcohol on the inhibition efficiency.

2.3 Weight Loss Experiment

A weight loss experiment is a simple method to determine the corrosion rate (CR) of mild steel. The mild steel samples with rectangle shape (50 mm × 25 mm × 2 mm) were immersed in 1 mol L^{-1} HCl in the absence and presence of each of the studied corrosion inhibitors with different concentrations (from 0.001 to 0.1 mmol L^{-1}) for a period of 3 h at 298, 308, and 318 K. The inhibition performance (η_W %) and surface coverage (θ) were calculated using **Eqs. 1** and **2** (Singh et al., 2016):

$$\eta_W(\%) = \frac{CR_0 - CR}{CR_0} \times 100 \quad (1)$$

$$\theta = \frac{CR_0 - CR}{CR_0} \quad (2)$$

where CR_0 and CR are the CRs without and with different concentrations of DPIP and OPIP, respectively; θ is the degree of surface coverage of DPIP and OPIP.

2.4 Electrochemical Evaluation

The electrochemical measurements were carried out with an Ivium workstation; this device is connected to a cell with three electrodes: a working electrode (mild steel sample) with exposure area 1 cm^2, a reference electrode (saturated calomel electrode), and a counter electrode (platinum sheet). Before the electrochemical test, soak the working electrode in the test solution for 30 min to stabilize the corrosion potential. For potentiodynamic polarization study, the potential sweep ranges from −600 to −100 mV (*vs.* SCE) with a scan rate of 0.5 mV s^{-1}. Electrochemical parameters such as corrosion potential (E_{corr}), corrosion current densities (i_{corr}), and Tafel slopes (β_c, β_a) can be derived by extrapolation of the linear Tafel segments of the polarization curves. Electrochemical impedance spectroscopy (EIS) tests were made in the frequency range of 10^5–0.01 Hz with an excitation signal of 10 mV.

2.5 Mild Steel Surface Analyses

Corroded mild steel surface obtained after 3 h immersion in the HCl solution with and without the optimal concentration of 0.1 mmol L^{-1} inhibitors was analyzed using TESCAN VEGA three SBH scanning electron microscope. The accelerating voltage is 20 kV. AFM was done using a Bruker MULTIMODE eight instrument. AFM was conducted using a tapping mode and a 2.5 Hz scan rate. XPS spectra were obtained using the PHI5000-VersaProbe system using Mg Kα radiation as the excitation source.

2.6 Computational Details

2.6.1 Toxicity Prediction

First, the toxicity and solubility of DPIP and OPIP were predicted. The toxicity assessment was carried out in T.E.S.T. software, which is based on the quantitative structure–activity relationship (QSAR) model, a mathematical approach exploited to solve toxicity prediction in light of the physical characteristics of molecular structure (Raevsky et al., 2011).

2.6.2 DFT Calculations

The quantum chemical parameters were calculated by DFT using Gaussian 09W to analyze the corrosion inhibition mechanism of DPIP and OPIP. The optimized molecular structure and its molecular orbital [highest occupied molecular orbital (HOMO) and lowest unoccupied molecular orbital (LUMO)] were obtained by the b3lyp/6–31G method, which is considered an efficient and reliable method to deal with quantum chemical problems (Rahmani et al., 2019a). All parameters such as E_{HOMO}, E_{LUMO}, the energy gap ($\Delta E = E_{HOMO} - E_{LUMO}$), the dipole moment ($\mu$), and the fraction of electrons transferred (ΔN) of the studied compounds in neutral forms were calculated and discussed (El-Hajjaji et al., 2018).

The local reactivity of corrosion inhibitors can be acquired by analyzing the Fukui functions (Parr and Yang, 1984). The Fukui function f_k is defined as follows. N is the number of electrons, $\rho(r)$ is the electronic density, and $\nu(r)$ is the constant external potential (Khaled, 2010):

$$f_k = \left(\frac{\partial \rho(r)}{\partial N}\right)_{\nu(r)} \quad (3)$$

The Fukui function can be obtained by calculating the Milliken charges distribution of the atoms of a molecule.

The Fukui function is represented by finite difference approximations as follows:

$$f_k^+ = q_k(N+1) - q_k(N) \quad (\text{for nucleophilic attack}) \quad (4)$$

$$f_k^- = q_k(N) - q_k(N-1) \quad (\text{for electrophilic attack}) \quad (5)$$

where $q_k(N)$, q_k $(N + 1)$, and q_k $(N - 1)$ are the charges of the neutral, cationic, and anionic species, respectively. N is the number of electrons in the neutral species. In this work, Fukui functions for DPIP and OPIP were calculated with the Multiwfn software (Fan et al., 2015).

As it is known, the concept of generalized philicity has been introduced (Parthasarathi et al., 2004); they defined a local quantity called philicity associated with a site k in a molecule with the assistance of corresponding condensed-to-atom variants of Fukui function. The local softness $\sigma_k^{\pm}$ (σ_k^+ and σ_k^-) and electrophilicity $\omega_k^{\pm}$ (ω_k^+ and ω_k^-) are related to the electrophilic and nucleophilic attacks, respectively. Also, $\sigma_k^{\pm}$ and $\omega_k^{\pm}$ can be calculated according to **Eqs 6**, **7** (Lee et al., 1988).

$$\sigma_k^{\pm} = \sigma f_k^{\pm} \quad (6)$$

$$\omega_k^{\pm} = \omega f_k^{\pm} \quad (7)$$

where σ_k^+ and σ_k^- denote the local softness for the nucleophilic and electrophilic attacks, respectively. ω_k^+ and ω_k^- are the local electrophilicity for the nucleophilic and electrophilic attacks, respectively.

Further, it was affirmed that the dual local descriptors such as dual Fukui $\Delta f(k)$ (difference between the nucleophilic and electrophilic Fukui functions), dual local softness $\Delta\sigma_k$

(difference between the nucleophilic and electrophilic local softness), and the philicity $\Delta\omega_k$ (difference between the nucleophilic and electrophilic philicity functions) are more accurate and consistent tools than the aforementioned local reactivity indices (Morell et al., 2006; Padmanabhan et al., 2006). In addition, $\Delta f(k)$, $\Delta\sigma_k$, and $\Delta\omega_k$ are calculated according to the following **Eqs 8–10**.

$$\Delta f\,(\mathrm{k}) = f_k^{\pm} - f_k^{-} \tag{8}$$

$$\Delta\sigma_k = \sigma_k^{+} - \sigma_k^{-} \tag{9}$$

$$\Delta\omega_k = \omega_k^{+} - \omega_k^{-} \tag{10}$$

If $\Delta\omega_k$ (or $\Delta f(\mathrm{k})$) > 0, the site k is favored for a nucleophilic attack, whereas if $\Delta\omega_k$ (or $\Delta f(\mathrm{k})$) < 0, the site k may be favored for an electrophilic attack.

2.6.3 Molecular Dynamic Simulation Details

Molecular dynamic (MD) simulation is usually used to study the interaction and adsorption between corrosion inhibitors and metal surfaces. This method can better understand the molecular interaction mechanism of corrosion inhibitors (El Faydy et al., 2019; Laabaissi et al., 2019; Benhiba et al., 2020). In this work, the adsorption processes of DPIP and OPIP on mild steel surfaces were investigated by Materials Studio eight software. The simulation of the Fe (1 1 0) surface was implemented by placing the surface crystal in a cell (32.27 × 32.27 × 30.13 Å^3). The liquid phase contained 5 Cl^-, 5 H_3O^+, and 495 H_2O. A 40 Å vacuum layer was established on the liquid layer to avoid the interaction between the surface and periodic repeating planes. The simulations were implemented at 298 K controlled by NVT ensemble with Andersen thermostat. The simulation was performed by Forcite code in a COMPASS force field for 200 ps with a time step of 0.1 fs (Andersen, 1980; Sun, 1998). The diffusions of Cl^-, H_3O^+, and H_2O in the inhibitor membranes were also simulated.

3 RESULTS AND DISCUSSIONS

3.1 Toxicity of Inhibitors

Some important toxicity endpoints involving developmental toxicity potential (DTP) and mutagenicity (M) were chosen to represent the toxicities. Generally, predicted values from 0.00 to 0.50 represent low toxicity probabilities, while predicted values >0.50 indicate high toxicity probabilities. The LD_{50} value should be greater than 300 mg/kg (**Supplementary Table S1**) (Alhaffar, et al., 2019). With careful inspection of the obtained probability values in **Supplementary Figure S1**, we can affirm that the toxic level of DPIP and OPIP is in the safe area. The probability for biodegradability (B) is 0.595 and 0.610, respectively, which implies that this substance is biodegradable and environmentally friendly.

3.2 Weight Loss Measurement

The inhibitory performance of the studied imidazo pyrimidine derivatives was realized by the weight loss method after 3 h immersions in 1 mol L^{-1} HCl solution in the presence and absence of the corrosion inhibitors at different temperatures. **Table 1** gives the values of the CR and the inhibition efficiency (η_W %).

From **Table 1**, the results showed that DPIP and OPIP have good corrosion inhibition properties for mild steel in the 1 mol L^{-1} HCl solution. The anti-corrosion performance gets better with increase in inhibitor concentration. At a concentration of 0.1 mmol L^{-1}, the inhibition efficiency of OPIP and DPIP reached the maximum 94.1% and 93.4%, respectively. This may be because the corrosion process of mild steel in a corrosion solution could be retarded by the adsorption of corrosion inhibitor molecules on the mild steel surface. The high anti-corrosion property of DPIP and OPIP is probably explained by the adsorption of the electron-rich imidazo pyrimidine group and improved with the carbon chain on the benzene ring.

Table 1 clearly shows that the corrosion degree increases with the increase of temperature. The corrosion inhibition efficiency of DPIP and OPIP decreases, which can be interpreted to mean that organic corrosion inhibitor molecules are easier to desorb from the metal surface with the rise of temperature.

3.3 Potentiodynamic Polarization Study

The polarization curves without and with different concentrations of OPIP and DPIP in the 1 mol L^{-1} HCl solution at 298 K are presented in **Figure 2**. The electrochemical parameters are reported in **Table 2**.

By analyzing the cathodic and anodic polarization curves in **Figure 2**, the corrosion inhibitor has a significant impact on the anodic and cathodic processes of corrosion reaction after adding DPIP and OPIP. A decrease in the cathodic current densities can be explained by the reduction of the exposed surface area caused by the adsorption of inhibitor molecules which leads to a reduction of hydrogen evolution reaction, while the decrease in anodic current density is caused by reduced dissolution reaction of mild steel. The inhibition performance of DPIP and OPIP is related to the adsorption on the working electrode surface and the formation of the barrier film (Monticelli et al., 2019). It is well known that the reduction of hydrogen ions needs two consecutive steps (Singh and Quraishi, 2010; El-Taib Heakal et al., 2012). In this work, the cathodic curves conform to the form of the Tafel curve, and the hydrogen evolution reaction on the mild steel surface is carried out based on the pure activation mechanism.

There is no defined trend for the shift of E_{corr} value. However, if the E_{corr} value deviates more than ±85 mV from the blank E_{corr} value, the inhibitor can be classified as a cathodic or anodic inhibitor; otherwise, it can be regarded as a mixed inhibitor affecting cathodic reaction (hydrogen evolution) and anodic reaction (metal dissolution) (Anusuya et al., 2017; Haque et al., 2017; Ouici et al., 2017; Salhi et al., 2017). In this study, the addition of different concentrations of corrosion inhibitors will lead to a slight change in the E_{corr} value, which is no more than 85 mV compared with the blank E_{corr} value. Therefore, the undefined trend shift of E_{corr} for DPIP and OPIP showed a mixed inhibition behavior.

TABLE 1 | Weight loss data of the mild steel with DPIP and OPIP in 1 mol·L^{-1} HCl at different temperatures.

Inhibitor	C (mmol·L^{-1})	298K			308K			318K		
		Δw (mg)	CR (mg·cm^{-2}·h^{-1})	η_w (%)	Δw (mg)	CR (mg·cm^{-2}·h^{-1})	η_w (%)	Δw (mg)	CR (mg·cm^{-2}·h^{-1})	η_w (%)
Blank	0	62.4	0.91	—	70.9	1.04	—	76.3	1.12	—
DPIP	0.001	12.8	0.19	79.5	21.2	0.31	70.1	25.1	0.37	67.1
	0.005	11.4	0.17	81.7	18.8	0.27	73.5	23.4	0.34	69.3
	0.01	8.34	0.12	86.6	14.1	0.21	80.1	19.1	0.28	75.0
	0.05	6.13	0.09	90.2	10.7	0.16	84.9	16.8	0.25	78.0
	0.1	4.09	0.06	93.4	8.69	0.13	87.7	11.7	0.17	84.7
OPIP	0.001	13.1	0.19	79.0	20.5	0.30	71.1	25.2	0.37	67.0
	0.005	10.8	0.16	82.7	18.3	0.27	74.2	22.9	0.33	70.0
	0.01	7.59	0.11	87.8	13.2	0.19	81.4	19.2	0.28	74.8
	0.05	5.83	0.09	90.7	9.52	0.14	86.6	16.5	0.24	78.4
	0.1	3.71	0.05	94.1	7.91	0.12	88.8	11.5	0.16	85.6

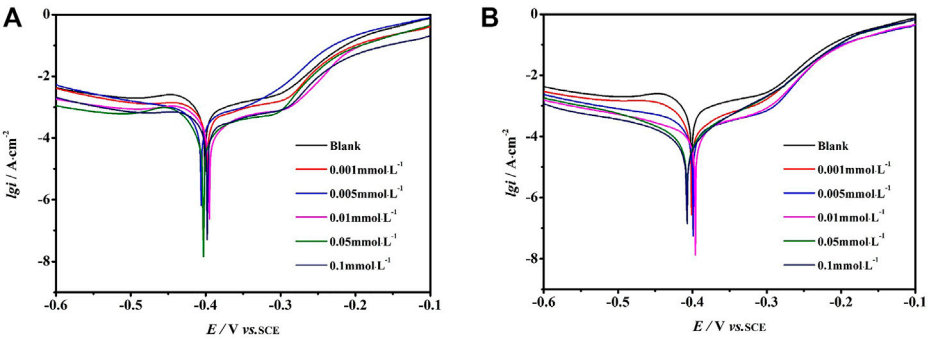

FIGURE 2 | Polarization curves for the mild steel in 1 mol L^{-1} HCl containing different concentrations of DPIP **(A)** and OPIP **(B)** at 298 K.

TABLE 2 | Polarization curve parameters of mild steel in 1 mol L^{-1} HCl with various concentrations of inhibitors (DPIP and PIP) at 298K.

Inhibitors	C (mmol·L^{-1})	-E_{corr} (mV)	β_a (mV·dec^{-1})	-β_c (mV·dec^{-1})	i_{corr} (μA·cm^{-2})	η_i (%)
Blank	0	401	151	178	735	—
DPIP	0.001	398	87	172	312	57.6
	0.005	406	89	163	222	69.8
	0.01	395	74	150	184	75.0
	0.05	403	75	155	143	80.5
	0.1	398	79	151	103	86.0
OPIP	0.001	403	83	174	302	58.9
	0.005	399	85	167	225	69.4
	0.01	396	81	154	186	74.7
	0.05	407	72	152	132	82.0
	0.1	409	78	143	97.5	86.7

The inhibition efficiencies calculated by the corrosion current density without and with inhibitors at different concentrations are shown in **Eq. 11**:

$$\eta_i(\%) = \frac{i^0_{corr} - i_{corr}}{i^0_{corr}} \times 100 \quad (11)$$

where i^0_{corr} and i_{corr} are the corrosion current density without and with DPIP and OPIP, respectively. The results give kinetic information of cathodic and anodic reactions. Also, the results match the weight loss method.

3.4 EIS Measurements

EIS was used to obtain information about the mechanism of charge transfer, diffusion, and adsorption between the electrode surface and the studied corrosion inhibitors. Nyquist diagrams of the mild steel immersed in 1 mol L^{-1} HCl without and with

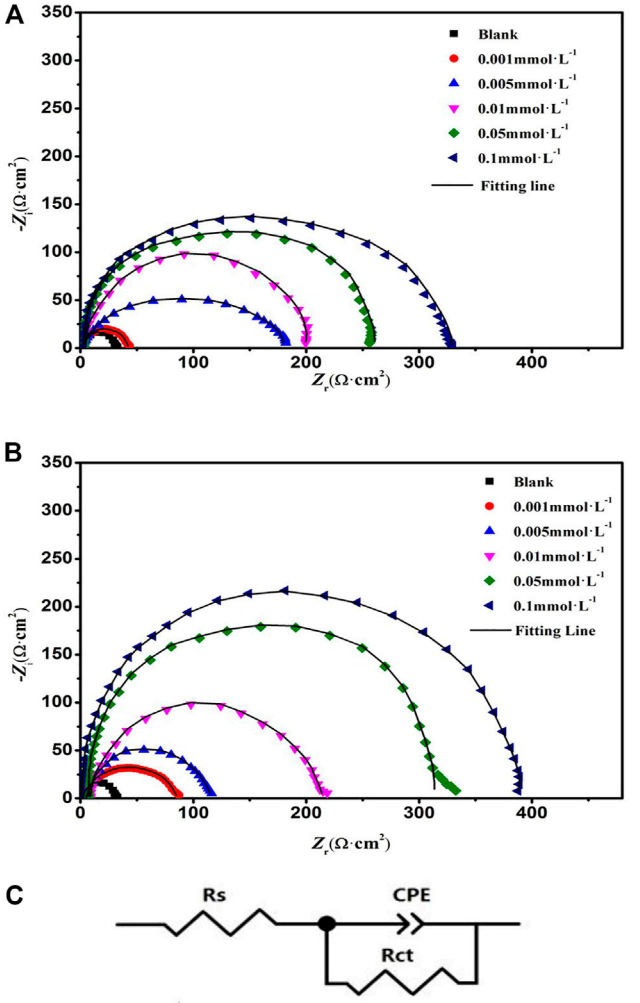

FIGURE 3 | Nyquist plots of DPIP **(A)**, OPIP **(B)** and equivalent circuit **(C)** for mild steel in 1 mol L^{-1} HCl containing different concentrations at 298K.

different concentrations of DPIP and OPIP are presented in **Figure 3**.

It is noted from the Nyquist graphs that the impedance spectra consist of single depressed semicircle capacitive loops, which are caused by the frequency dispersion and the heterogeneity of the electrode surface (Khadiri et al., 2018; El Faydy et al., 2018). The shape of impedance spectra obtained in different electrolyte solutions (containing different concentrations of corrosion inhibitor and blank) are the same, which suggests that the corrosion mechanism of mild steel has not changed, and the radius of capacitive loops increases significantly after increasing the corrosion inhibitor concentration. The behavior of the impedance can be illustrated by adapting an electrochemical equivalent circuit (**Figure 3**) including a solution resistance (R_s), constant phase element (*CPE*), and the charge transfer resistance (R_{ct}) (Pan et al., 2020). The electrochemical parameters are listed in **Table 3**.

CPE values are calculated using **Eq. 12** (Zhang et al., 2012):

$$Z_{CPE} = Q^{-1}(iw)^{-n} \tag{12}$$

where Q, w, i, and n stand for *CPE* constant, the angular frequency, imaginary root, and the deviation indicator related to the homogeneity of the work electrode surface, respectively. In addition, double-layer capacitance (C_{dl}) values are defined using **Eq. 13** (Brug et al., 1984):

$$c_{dl} = Q^{1/n}\left(\frac{R_s R_{ct}}{R_s + R_{ct}}\right)^{(1-n)/n} \tag{13}$$

The inhibition efficiency was evaluated using the following expression:

$$\eta_R(\%) = \frac{R_{ct} - R_{ct}^0}{R_{ct}} \times 100 \tag{14}$$

where R_{ct}^0 and R_{ct} mean the charge transfer resistance of blank electrolyte and electrolyte with inhibitors, respectively.

It is observed that the highest R_{ct} [329.2 ($\Omega\cdot cm^2$) for DPIP and 387.8 ($\Omega\cdot cm^2$) for OPIP] has been obtained at 0.1 mmol L^{-1}. With the increase of inhibitor concentration in the corrosive medium, the adsorption of inhibitor molecules on the surface of mild steel increases, which means that the exposed surface area of mild steel decreases, the charge transfer resistance increases, and the inhibition efficiency improves. On the other hand, the increase of R_{ct} value coincides with the decrease of C_{dl} value of the inhibitors, which can be explained as replacing Cl^- ions and H_2O molecules from the mild steel surface with inhibitor molecules. This process reduced the surface reaction of mild steel in the corrosive medium, increasing the resistance to charge and mass transfer (McCafferty and Hackerman, 1972).

3.5 Adsorption Studies

The adsorption isotherm gives the chance to better understand the interaction between the inhibitor molecules and the metal surface. Langmuir, Temkin, Freundlich, Flory Huggins, and El Awady adsorption isotherms (**Eqs 15–20**) are employed to obtain more information about adsorption behavior and the relationship between surface coverage and inhibitor concentration. The values of surface coverage are obtained from the weight loss data.

$$\frac{C}{\theta} = \frac{1}{K_{ads}} + C \quad \text{Langmuir} \tag{15}$$

$$\ln\left(\frac{\theta}{1-\theta}\right) = \ln K + y \ln C \ \ (K_{ads} = K^{1/y}) \quad \text{El} - \text{Awady} \tag{16}$$

$$\mathrm{n}\left(\frac{\theta}{C}\right) = \ln K_{ads} + x \ln(1-\theta) \quad \text{Flory} - \text{Huggins} \tag{17}$$

$$\ln\theta = \ln K_{ads} + Z \ln C \quad \text{Freundlich} \tag{18}$$

$$\ln\left[\left(\frac{\theta}{1-\theta}\right) \times \left(\frac{1}{C}\right)\right] = -\ln K_{ads} + 2d\theta \quad \text{Frumkin} \tag{19}$$

$$\theta = -\frac{1}{2a}\ln K_{ads} - \frac{1}{2a}\ln C \quad \text{Temkin} \tag{20}$$

Analysis of the different isotherms shows that the fitting provided by the Langmuir isotherm has a regression coefficient R^2 of 0.999 for DPIP and OPIP at 298 K

TABLE 3 | EIS parameters of mild steel in 1 mol L^{-1} HCl containing various concentrations of DPIP and OPIP.

Inhibitors	C (mmol·L^{-1})	R_s (Ω·cm^2)	CPE_{dl}		R_{ct} (Ω·cm^2)	η_R (%)
			C_{dl} (μF·cm^{-2})	n		
Blank	0	2.485	446	0.89	31.2	—
DPIP	0.001	2.571	338.4	0.88	43.4	28.1
	0.005	2.978	287.6	0.85	180.5	82.7
	0.01	2.764	203.8	0.86	199.8	84.4
	0.05	2.756	153.8	0.88	256.5	87.8
	0.1	2.525	112.5	0.88	329.2	90.5
OPIP	0.001	2.144	288.9	0.83	85.9	63.7
	0.005	2.426	267.2	0.86	116.4	73.2
	0.01	2.518	213.8	0.85	211.6	85.3
	0.05	2.913	123.1	0.85	327.6	90.5
	0.1	2.651	108.5	0.80	387.8	91.9

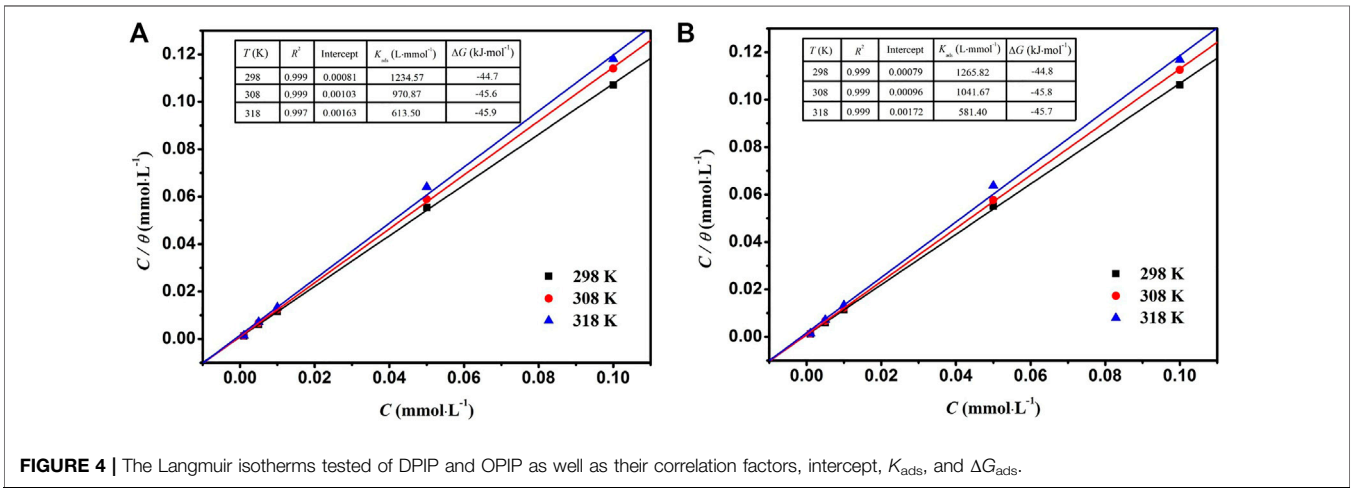

FIGURE 4 | The Langmuir isotherms tested of DPIP and OPIP as well as their correlation factors, intercept, K_{ads}, and ΔG_{ads}.

(**Figure 4**). The slope of the adsorption isotherm equation is slightly greater than 1 due to the inhomogeneity of the surface.

The values of the adsorption equilibrium constant K_{ads} can be accessed from the values of the standard free adsorption energies ΔG_{ads} by the following equality (Zhao et al., 2020):

$$\Delta G_{ads} = -RT \ln(55.5 \times K_{ads}) \tag{21}$$

where C_{H2O} is 55.5 mol L^{-1} in the solution; R is the constant of gases, and T is the temperature.

As we all know, if the value of ΔG_{ads} is near −20 kJ mol^{-1} or more positive, it can be regarded as physical adsorption. However, when the value of ΔG_{ads} is equal to or less than −40 kJ mol^{-1}, it is thought to be chemisorption through the interaction between lone pair electrons in inhibitor molecules and metal surface (Nahle et al., 2018; Rahmani et al., 2019b; Farhadian et al., 2021). In the present work, the values of ΔG_{ads} are less than −40 kJ mol^{-1}, which shows that the inhibitor molecules are adsorbed on the mild steel surface by strong chemical bonds. Chemical bindings with Fe unfilled orbitals are through the combination of donating lone electron pairs and/or π-electrons of the DPIP and OPIP molecules and Fe empty orbitals (chemical adsorption).

3.6 Thermodynamic Activation Parameters for DPIP and OPIP

From the weight loss measurement, the inhibitory performance decreased with rising temperature, so in this part, the effort of temperature on the inhibition performance of DPIP and OPIP was studied. The corrosion kinetic process of mild steel in the corrosive solution without and with inhibitors was described by the Arrhenius equation as follows (Khadraoui et al., 2016):

$$CR = k \exp\left(\frac{-E_a}{RT}\right) \tag{22}$$

where k is the frequency factor and E_a is the activation energy. The value of E_a of metal dissolution in the inhibitor-free or inhibitor-containing solution is based on the slope ($-E_a/R$) of the plot of lnCR~1/T (**Figure 5**).

The thermodynamic parameters such as enthalpy and entropy were described by the transition state equation (Khadraoui et al., 2016):

$$CR = \frac{RT}{N_a h} \exp\left(\frac{\Delta S}{R}\right) \exp\left(\frac{-\Delta H}{RT}\right) \tag{23}$$

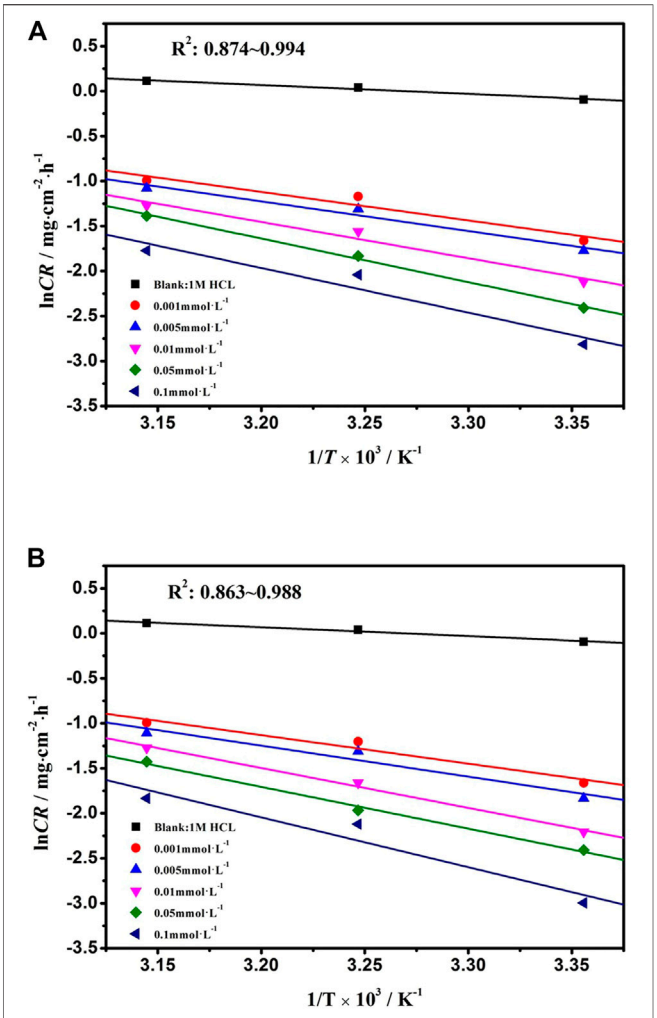

FIGURE 5 | ln*CR* versus 1,000/T for mild steel corrosion in 1 mol L^{-1} HCl with various concentrations of DPIP and OPIP.

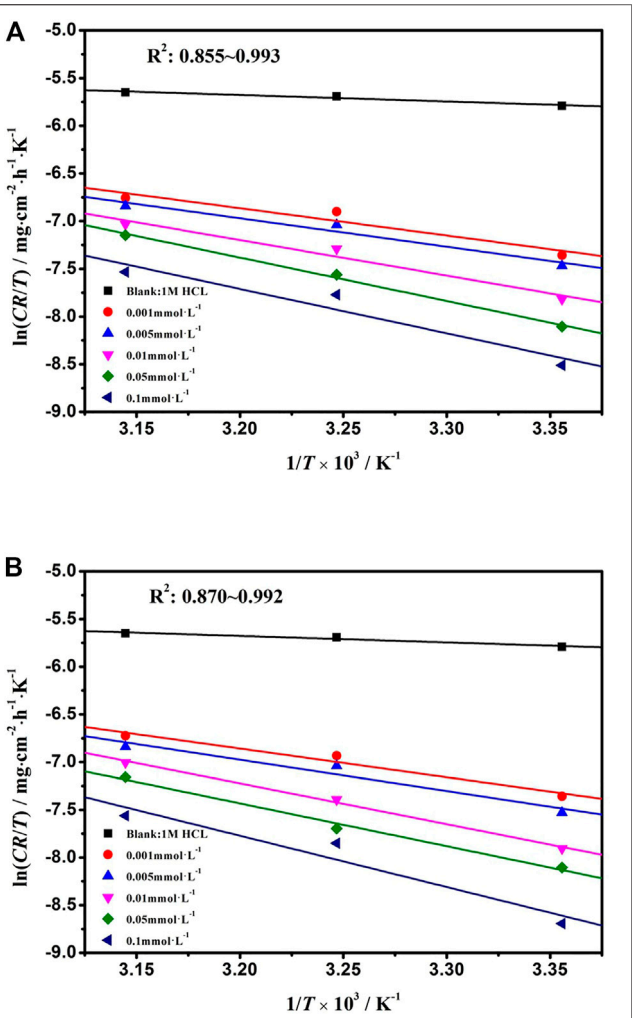

FIGURE 6 | ln [*CR*/*T*] versus 1,000/T for mild steel corrosion in 1 mol L^{-1} HCl with various concentrations of DPIP and OPIP.

where ΔH, ΔS, N_a, and h are enthalpy, entropy, Avogadro number, and Planck's constant, respectively. The relationship of ln [*CR*/*T*] ~ 1/*T* is showed in **Figure 6**. The values of ΔH and ΔS were obtained with the slope and intercept of the fitted line. The corrosion kinetic process of mild steel in the absent or present inhibitors solutions was described by the Arrhenius equation. The values of ΔH, ΔS, and E_a are listed in **Table 4**.

As showed in **Table 4**, the value of E_a for the mild steel in the inhibited solution is higher than that obtained for the uninhibited solution. The value of E_a in the inhibited solution (at least 26.38 kJ mol^{-1} for DPIP and 26.35 kJ mol^{-1} for OPIP) is higher than that in the blank solution and is 8.2 kJ mol^{-1}. It is well known that a higher value of the E_a than without inhibitors means that the inhibitors offer a thin adsorption film on the mild steel surface that creates a physical barrier for charge and mass transfer (Kannan et al., 2014). In addition, the activation energy was augmented with the increased inhibitors concentration, indicating that the dissolution rate of mild steel decreased in the corrosive medium (Sliem et al., 2019). The positive value of ΔH reflects that the dissolution process of mild steel in the studied solution is endothermic. Moreover, the difference between E_a and ΔH being greater than 0 also showed that gaseous reduction reaction (hydrogen evolution) occurred in the corrosion process (Zhang et al., 2021). Further analysis found that the average value of $E_a - \Delta H$ is about 2.56 kJ mol^{-1}, which is basically consistent with the value of RT (2.57 kJ mol^{-1}), indicating that the corrosion process is a unimolecular reaction (Gomma and Wahdan, 1995). Negative values of ΔS indicate the decrease in disorder. The adsorption process goes from the reagents to the activated complex, and complex compound formation was associated with the rate-determining step (Saady et al., 2021).

3.7 Surface Characterizations

3.7.1 SEM Analysis

SEM analysis provides two-dimensional visual information about the corrosion resistance of inhibitors to metal, which is a powerful supplement to the results of weight loss analysis and electrochemical

TABLE 4 | Activation parameters values in the nonexistence and existence of DPIP and OPIP solution.

Inhibitors	C (mmol·L^{-1})	ΔH (kJ·mol^{-1})	ΔS (J·mol^{-1}·K^{-1})	E_a (kJ·mol^{-1})	E_a-dh (kJ·mol^{-1})
Blank	0	5.64	−226.68	8.20	2.56
DPIP	0.001	23.82	−178.39	26.38	2.56
	0.005	24.84	−176.01	27.39	2.56
	0.01	30.92	−158.43	33.48	2.56
	0.05	37.73	−138.19	40.29	2.56
	0.1	38.67	−137.90	41.23	2.56
OPIP	0.001	25.04	−174.44	26.35	2.56
	0.005	27.33	−168.07	28.65	2.56
	0.01	35.55	−143.84	36.86	2.56
	0.05	37.27	−140.08	38.58	2.56
	0.1	44.74	−118.98	46.05	2.56

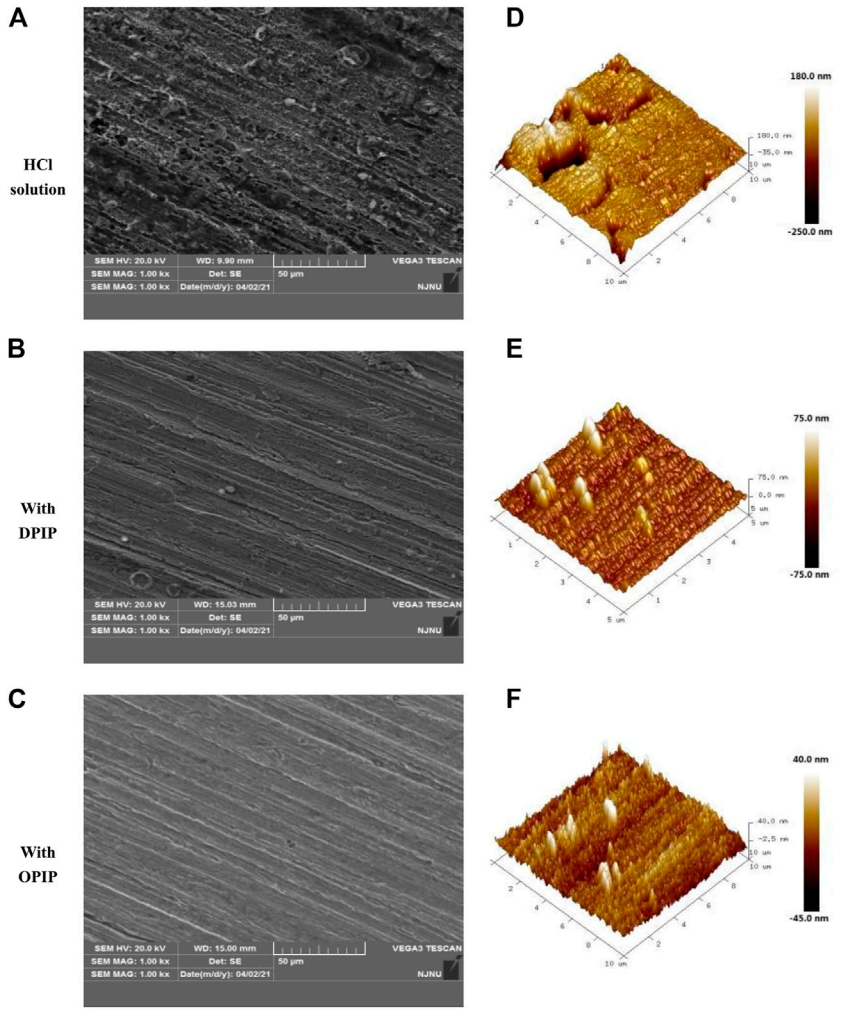

FIGURE 7 | SEM **(A–C)** and AFM **(D–F)** images of mild steel in 1 mol L^{-1} HCl without and with 0.1 mmol L^{-1} DPIP/OPIP after 3 h immersion.

research. The morphology of mild steel immersed in 1 mol L^{-1} HCl acid solution without and with 0.1 mmol L^{-1} of DPIP/OPIP for 3 h was studied, as showed in **Figures 7A–C**.

It is clear from **Figure 7** that the surface of mild steel is seriously damaged in the uninhibited acidic solution, reflecting a strong metal dissolution. The surface of mild

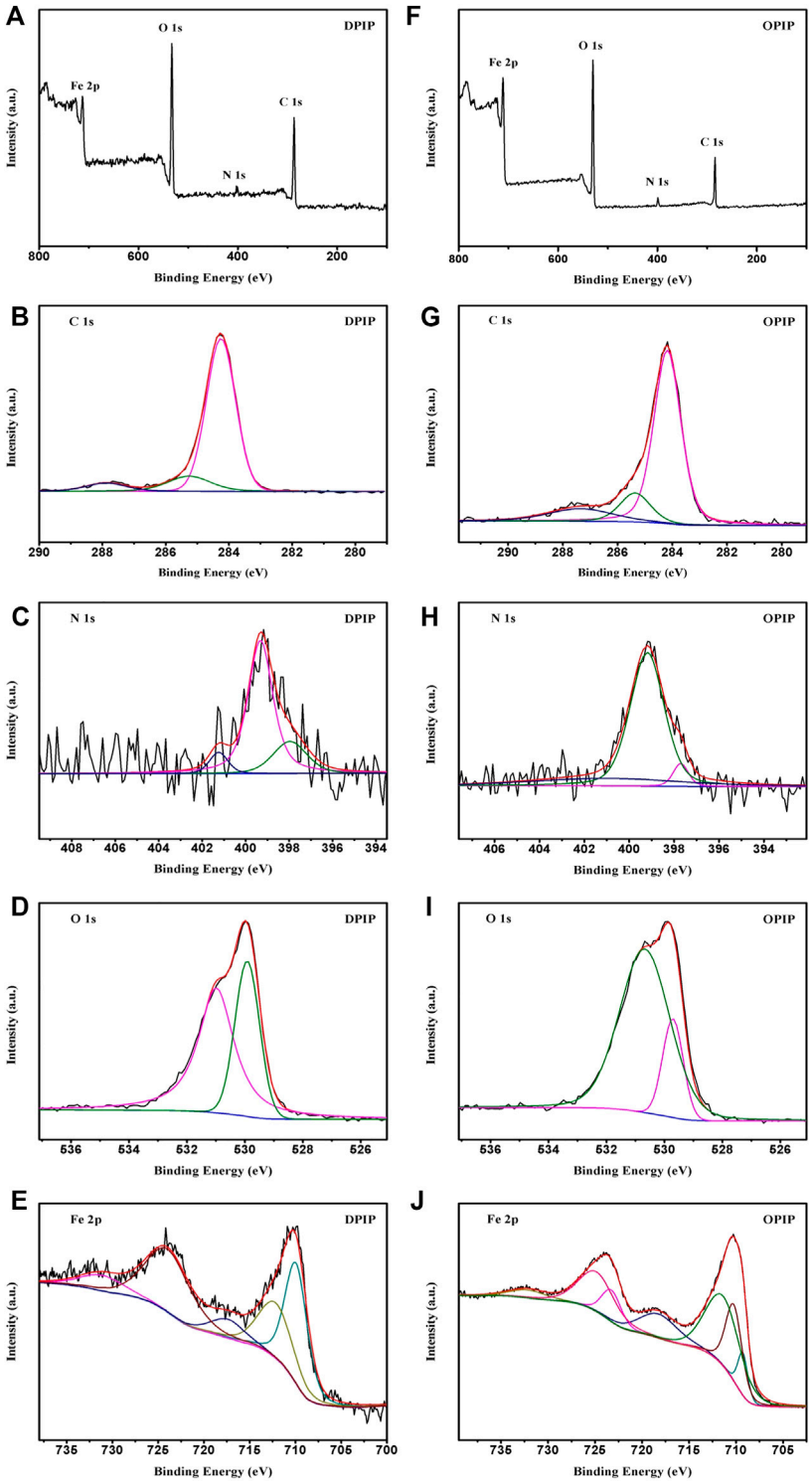

FIGURE 8 | XPS spectra of mild steel surface in 1 mol L^{-1} HCl without and with 0.1 mmol L^{-1} DPIP/OPIP after 3 h immersion: wide spectra, C 1s, N 1s, O 1s, and Fe 2p.

steel is rough and porous, and the hole is wide and deep. After adding DPIP/OPIP in the corrosive environment, the inhibitor molecules are adsorbed on the metal surface and cover the exposed surface to decrease the contact between the corrosive medium and the metal and delay the dissolution of the sample.

3.7.2 AFM Analysis

With the rapid development of high-resolution spatial characterization technology, AFM has been successfully implemented in the field of corrosion and protection. **Figure 7** shows the 3D morphology and roughness of mild steel surface with and without corrosion inhibitors in 1 mol L^{-1} HCl acidic medium. As shown in the figures, the surface of mild steel sample without corrosion inhibitor shows serious damage, with an average roughness of 33.7 nm. Compared with the sample without corrosion inhibitors, the metal surface of the sample with corrosion inhibitors is more uniform, and its roughness (RA) is lower. The average roughness of mild steel soaked in DPIP and OPIP solutions is 11 and 12 nm, respectively. AFM morphology further confirmed that the existence of corrosion inhibitors can effectively inhibit the corrosion of mild steel.

3.7.3 XPS Analysis

The composition of organic adsorption layer on mild steel surface in 1 mol L^{-1} hydrochloric acid corrosion medium with corrosion inhibitors was studied by XPS. The results demonstrate that the surface film is generally composed of ferric oxide and carbonaceous organic matter. In this way, the high-resolution peaks for C 1s, O 1s, N 1s, and Fe 2p for mild steel surface after 3 h of immersion in 1 mol L^{-1} HCl solution containing 0.1 mmol L^{-1} of DPIP and OPIP are recorded and shown in **Figure 8**.

The C 1s spectra of DPIP and OPIP show three peaks (287.9, 285.3, and 284.3) and (287.4, 285.4, and 284.2), respectively. The largest peak can be ascribed to the C–C and C=C aromatic bonds with the characteristic binding energy of 284.3 eV, with the peak at 284.2 eV in OPIP as well. Peaks at 285.3 or 285.4 eV referred to the C–H, and those at 287.9 or 287.4 eV referred to the C–N and C=N, respectively (Wagner et al., 1979; Watts and Wolstenholme, 2003; Yamashita and Hayes, 2008). The O 1s spectrum envelops were fitted by two peaks. The first peak located at 529.9 eV was attributed to Fe_2O_3 and/or Fe_3O_4 oxides. The second peak located at 530.8 eV (530.7 eV for OPIP) is attributed to the oxygen in hydrous iron oxides, such as FeOOH and/or $Fe(OH)_3$ (Temesghen and Sherwood, 2002). The peaks of the N 1s of the steel sample treated by DPIP may be fitted into three peaks located at 401.3, 399.3, and 398.0 eV corresponding to the quaternary nitrogen ($=N^+$-) atom of the imidazo pyrimidine ring (Tang et al., 2013), coordinated nitrogen atom, and C-N-metal bond (Weng et al., 1995; Finsgar et al., 2009), respectively. In the case of OPIP, these peaks are noted at 401.1, 399.2, and 397.7 eV.

The Fe 2p spectra were fitted to two doublets, 711.7 eV or 712.7 (Fe 2p3/2) and 724.3 eV or 724.6 (Fe 2p1/2), with an associated ghost structure. The peak is attributable to the Fe–N, which is reported to appear at 710.3 eV (711.7 eV for OPIP) (Ciampi and Di castro, 1995; Zhang et al., 2016). The peak located at 711.7 or 712.7 eV was assigned to ferric compounds such as FeOOH (i.e., oxyhydroxide), Fe_2O_3 (i.e., Fe^{3+} oxide), and/or Fe_3O_4 (i.e., Fe^{2+}/Fe^{3+} mixed oxide) (Pech-Canul and Bartolo-Perez, 2004; Bouanis et al., 2009); the peak observed at 718.6 or 718.7 eV may be ascribed to the satellite of Fe(III) (Ciampi and Di castro, 1995). Based on the previous observations, the XPS results support the presence of adsorbed inhibitors on the mild steel surface.

3.8 Quantum Chemical Calculations

3.8.1 DFT

Quantum chemistry research is often used to determine the correlation between the molecular structure and anti-corrosion performance of corrosion inhibitors (Zhao et al., 2014). DFT is a very powerful tool for calculating molecular electron descriptors and analyzing inhibitor/surface interaction. In this work, the HOMO and the LUMO were obtained by using Gaussian 09 software and given in **Figures 9A**–F (Xia et al., 2020).

It is worth noting that the frontier molecular orbitals of inhibitor molecules play a major role in predicting the contribution and acceptance of electrons. **Figure 9** shows that HOMO and LUMO orbitals of DPIP and OPIP molecules are distributed on the surfaces of pyrimidine and imidazole parts. It can be noted that heteroatoms, such as N atoms, and benzene rings related to the above groups are very active. This means that the above sites are more involved in the inhibitor–metal interaction in the donor–acceptor process (Qiang et al., 2017). In addition to graphical representation, different quantum chemical parameters such as E_{HOMO}, E_{LUMO} ΔE, and ΔN were calculated to further explain the reactivity of corrosion inhibitors and their adsorption capacity on mild steel surface. **Table 5** summarizes the most important quantum chemical descriptors obtained after geometry optimization in the neutral form for each molecule in the aqueous phase.

Generally speaking, the reactivity of inhibitor molecules can be forecast by the energy of molecular orbitals: high HOMO energy represents the tendency of molecules to give electrons, and high LUMO energy represents the tendency to accept electrons. Therefore, the corrosion inhibitor with higher HOMO and the lower LUMO energy can be expected to have high anti-corrosion performance. In this work, it can be seen that the HOMO energy of OPIP is higher than that of DPIP, which has a stronger electron supplying ability, while the LUMO orbital energy of DPIP is higher, which shows a stronger electron receiving ability. This result cannot directly be used to judge the anti-corrosion performance of the corrosion inhibitors but also needs to be compared through the energy gap of the molecule. The corrosion inhibitor with high reaction activity has a lower value of energy gap (Kozlica et al., 2021).

From **Table 5**, The ΔE values of OPIP (3.528 eV) is lower than DPIP (3.534 eV), indicating that OPIP molecules are more likely to react with the mild steel surface.

In addition, the dipole moment of OPIP (6.166 D) is also higher than DPIP (6.099), reflecting a better reactivity, which is well correlated to the ΔE. On the other hand, Lukovits have found theoretically that If $\Delta N < 3.6$, ΔN indicates the ability to provide electrons to the metal surface (Lukovits et al., 2001; Qiang et al., 2018). In the present work, the ΔN values of the corrosion inhibitors studied are less than 3.6, which indicates that the molecules of the inhibitors are the electron donor and the metal surface is an acceptor.

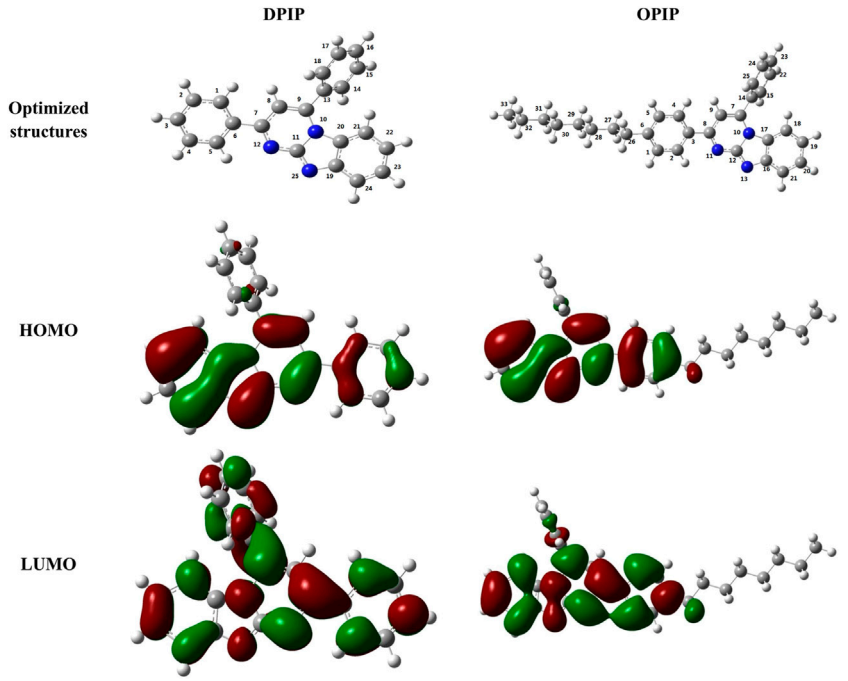

FIGURE 9 | Optimized structures, HOMO, and LUMO of DPIP and OPIP molecules obtained at B3LYP/6–31G level in aqueous solution.

TABLE 5 | Quantum chemical descriptors and MD data of DPIP and OPIP.

Inhibitors	E_{HOMO} (eV)	E_{LUMO} (eV)	ΔE (eV)	μ (D)	ΔN	$E_{interaction}$ (kJ·mol^{-1})	$E_{binding}$ (kJ·mol^{-1})
DPIP	−5.587	−2.053	3.534	6.099	0.2830	−534.67	534.67
OPIP	−5.518	−1.990	3.528	6.166	0.3022	−593.25	593.25

3.8.2 Fukui Index

Fukui index was used to understand the reactivity of DPIP and OPIP inhibitor molecules by identifying the electrophilic and nucleophilic attack sites (f_k^+ and f_k^-). **Supplementary Table S2** shows the Fukui index of corrosion inhibitors in an optimized form calculated in the neutral state in the aqueous phases.

It can be observed that the inhibitor molecule has multiple active donor–acceptors. The preferred sites for electrophilic attacks of the two inhibitors are found mainly on the benzene ring, imidazo ring, and pyrimidine ring, while the preferred sites for nucleophilic attacks are located on the imidazo ring and pyrimidine ring. According to the analysis above, the imidazo [1,2 a] pyrimidine group could be the main reactive site, which suggests that the imidazo [1,2 a] pyrimidine group has a stronger tendency to donate electrons to Fe^{2+} or Fe^{3+} on the Fe (110) surface. This indicates that these sites are liable to be the preferred sites for corrosion inhibitor molecules to adsorb on the mild steel surface.

Further, instead of analyzing the data of the Fukui functions ((f_k^+ and f_k^-), the local softness ($\sigma_k^{\pm}$), and the electrophilicity ($\omega_k^{\pm}$), the results of the dual Fukui function (Δf_k), the dual local softness ($\Delta\sigma_k$), and the dual local philicity ($\Delta\omega_k$) are analyzed and investigated; the graphical representation of the dual local descriptors (Δf_k, $\Delta\sigma_k$, and $\Delta\omega_k$) of the most representative active sites are presented in **Supplementary Figure S2** and **Supplementary Table S2**.

It was reported that if the dual local descriptors (Δf_k, $\Delta\sigma_k$, and $\Delta\omega_k$) are less than 0, the process is favored for an electrophilic attack; however, if (Δf_k, $\Delta\sigma_k$, and $\Delta\omega_k$) > 0, the process is favored for a nucleophilic attack (Geerlings et al., 2012). As results in **Supplementary Table S2** show, the three descriptors Δf_k, $\Delta\sigma_k$, and $\Delta\omega_k$ are lower than 0, which suggests that the two corrosion inhibitors studied have many active centers and have the ability to accept electrons from the metal, while the sites with the Δf_k, $\Delta\sigma_k$, and $\Delta\omega_k$ higher than 0 suggest electrophilic centers (Cuan et al., 2005; Domingo et al., 2016). As results in **Supplementary Table S2** show, the most active sites for electron accepting centers for DPIP and OPIP have the following trend: C14 > C6 > C2 > C17 > C18 > C19 > C24 > C20 > C22 > C11 > C9 > N25 > N10 > N12 > C21 > C8 > C7 > C13 and C14 > C6 > C2 > C17 > C18 > C26 > C19 > C24 > C20 > C22 > N11 > C9 > C25 > N10 > C12 > C21 > C8 > C7 > N13, respectively. However, the most active sites donating active centers for DPIP and OPIP can be arranged as follows: C5 > C3 > C1 > C23 > C15 > C16 > C4 and C5 > C3 > C28 > C1 > C29 > C30 > C27 > C31 > C32 > C33 > C23 > C15 > C16 > C4, respectively.

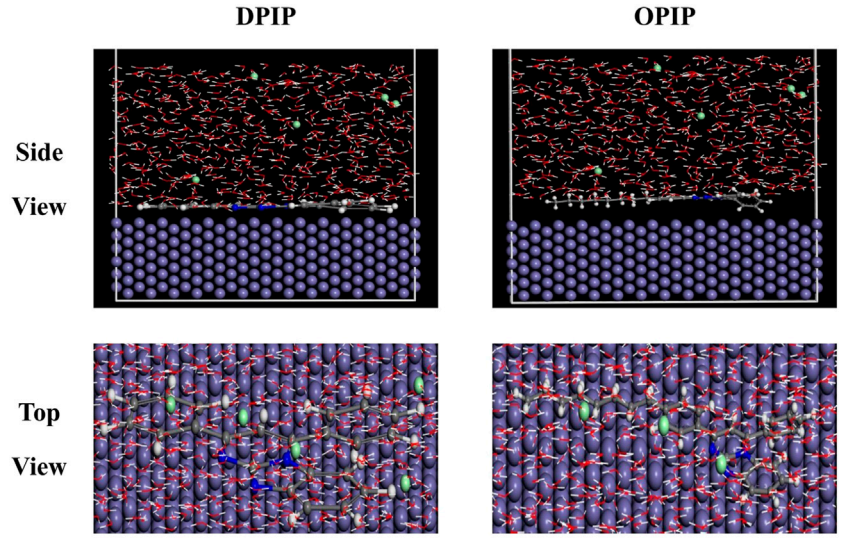

FIGURE 10 | Top and side views of the stable adsorption configuration of DPIP **(A)** and OPIP **(B)** obtained by molecular dynamic simulations on Fe (110).

3.9 MD Simulation Results

The performances of the studied molecules to the migration of corrosive species like Cl^-, H_3O^+, and H_2O are investigated with the help of diffusion coefficient values. The MSD is a microscopic parameter that is involved, defined as:

$$MSD(t) = \left[\frac{1}{N}\sum_{i=1}^{N}|R_i(t) - R_i(0)|^2\right] \quad (24)$$

$$D = \frac{1}{6}\lim_{t\to\infty}\frac{d}{dx}\sum_{i}^{N}\left[|R_i(t) - R_i(0)|^2\right] \quad (25)$$

where $|R_i(t) - R_i(0)|^2$ and N represents the MSD number of target molecules, respectively. The positions of corrosive particles at time t and 0 are given by $R_i(t)$ and R_i (0), respectively.

The MSD curves of Cl^-, H_3O^+, and H_2O in the protective film of DPIP and OPIP are shown in **Supplementary Figure S3**. The magnitude of diffusion coefficients for Cl^-, H_3O^+, and H_2O are 0.3222, 0.7830, and 2.3920 × 10^{-9} m^2/s, respectively (Ehteshamzade et al., 2006). However, the calculated diffusion coefficients for Cl^-, H_3O^+, and H_2O decrease significantly in the film of DPIP and OPIP (**Supplementary Table S3**). This observation reveals that the addition of DPIP and OPIP into the corrosive media generates a protective film over the mild steel surface and creates hindrance in the migration of corrosive species. The reduction in the diffusion coefficient values of OPIP is higher as compared to DPIP, which suggests more protective film formation in the case of OPIP over the metal surface than DPIP. This result further reinforces the superior performance of OPIP than DPIP and supports the experimental finding.

Figure 10 gives the top and side views of the stable adsorption configuration of DPIP and OPIP molecules on the Fe (1 1 0) surface in the presence of chloride ions with the temperatures of 298 K. It can be seen from the figure that the molecules of DPIP and OPIP are adsorbed on the Fe (1 1 0) surface in parallel in the presence of H_2O, H_3O, and Cl^-. This is due to a high number of active electron donor units in the imidazopyrimidine group, which is easier to adsorb with surface atoms on the mild steel substrate (Hsissou et al., 2020).

The interaction energy ($E_{interaction}$) and adsorption energy ($E_{binding}$) are employed to measure the interaction and adsorption capacity of DPIP and OPIP with the very fine surface of Fe (1 1 0), respectively. $E_{interaction}$ and $E_{binding}$ values are calculated according to the following two equations and listed in **Table 5** (Asadi et al., 2019):

$$E_{interaction} = E_{total} - (E_{surface+solution} + E_{inhibitor}) \quad (26)$$

$$E_{binding} = -E_{interaction} \quad (27)$$

The high absolute value of interaction and binding energy indicates the ability to replace the corrosive ions and H_2O molecules to form a protective layer against the corrosive medium (Guo et al., 2017; Rbaa et al., 2019). In this work, the interactions with the Fe (1 1 0)/OPIP interface are greater compared to interactions with the Fe (1 1 0)/DPIP interface, which is due to the carbon chain effect, so that leads to an increase in interactions at the interface. The data in **Table 5** show that the $E_{binding}$ value of OPIP is higher than that of DPIP, indicating the higher adsorption capacity of the compound.

4 CONCLUSION

The use of corrosion inhibitors is one of the important methods for surface modification of mild steel to prevent

corrosion. The synthesized DPIP and OPIP have high corrosion inhibition performance for mild steel in 1 mol L^{-1} HCl solution. Electrochemical test results show that the inhibition efficiency increases with increasing concentration. Both the inhibitors are mixed-type inhibitors in 1 mol L^{-1} HCl solution, and EIS data showed that the corrosion inhibitors played their role by adsorption on the mild steel surface. The adsorption of DPIP and OPIP on the mild steel obeys the Langmuir adsorption isotherm model. The addition of inhibitors leads to an increase in the activation energy of corrosion, indicating that the inhibitor adsorption on the metallic surface increased the energy barrier for the corrosion process. The theoretical calculations by the DFT method reveal that the adsorption of DPIP and OPIP is a chemical adsorption mainly through the bonding of N atoms or aromatic ring to the Fe surface, which is supported by MD simulation.

DATA AVAILABILITY STATEMENT

The original contributions presented in the study are included in the article/**Supplementary Material**, further inquiries can be directed to the corresponding author.

AUTHOR CONTRIBUTIONS

All authors listed have made a substantial, direct, and intellectual contribution to the work and approved it for publication.

SUPPLEMENTARY MATERIAL

The Supplementary Material for this article can be found online at: https://www.frontiersin.org/articles/10.3389/fmats.2022.843522/full#supplementary-material

REFERENCES

Alhaffar, M. T., Umoren, S. A., Obot, I. B., Ali, S. A., and Solomon, M. M. (2019). Studies of the Anticorrosion Property of a Newly Synthesized Green Isoxazolidine for API 5L X60 Steel in Acid Environment. *J. Mater. Res. Techn.* 8, 4399–4416. doi:10.1016/j.jmrt.2019.07.051

Andersen, H. C. (1980). Molecular Dynamics Simulations at Constant Pressure And/or Temperature. *J. Chem. Phys.* 72, 2384–2393. doi:10.1063/1.439486

Anejjar, A., Salghi, R., Zarrouk, A., Zarrok, H., Benali, O., Hammouti, B., et al. (2015). Investigation of Inhibition by 6-Bromo-3-Nitroso-2-Phenylimidazol [1,2-A]pyridine of the Corrosion of C38 Steel in 1 M HCl. *Res. Chem. Intermed* 41, 913–925. doi:10.1007/s11164-013-1244-7

Anusuya, N., Saranya, J., Sounthari, P., Zarrouk, A., and Chitra, S. (2017). Corrosion Inhibition and Adsorption Behaviour of Some Bis-Pyrimidine Derivatives on Mild Steel in Acidic Medium. *J. Mol. Liquids* 225, 406–417. doi:10.1016/j.molliq.2016.11.015

Asadi, N., Ramezanzadeh, M., Bahlakeh, G., and Ramezanzadeh, B. (2019). Utilizing Lemon Balm Extract as an Effective green Corrosion Inhibitor for Mild Steel in 1M HCl Solution: a Detailed Experimental, Molecular Dynamics, Monte Carlo and Quantum Mechanics Study. *J. Taiwan Inst. Chem. Eng.* 95, 252–272. doi:10.1016/j.jtice.2018.07.011

Benhiba, F., Serrar, H., Hsissou, R., Guenbour, A., Bellaouchou, A., Tabyaoui, M., et al. (2020). Tetrahydropyrimido-Triazepine Derivatives as Anti-corrosion Additives for Acid Corrosion: Chemical, Electrochemical, Surface and Theoretical Studies. *Chem. Phys. Lett.* 743, 137181. doi:10.1016/j.cplett.2020.137181

Bouanis, F. Z., Bentiss, F., Traisnel, M., and Jama, C. (2009). Enhanced Corrosion Resistance Properties of Radiofrequency Cold Plasma Nitrided Carbon Steel: Gravimetric and Electrochemical Results. *Electrochimica Acta* 54, 2371–2378. doi:10.1016/j.electacta.2008.10.068

Brug, G. J., Van Den Eeden, A. L. G., Sluyters-Rehbach, M., and Sluyters, J. H. (1984). The Analysis of Electrode Impedances Complicated by the Presence of a Constant Phase Element. *J. Electroanalytical Chem. Interfacial Electrochemistry* 176, 275–295. doi:10.1016/0368-1874(84)83477-210.1016/s0022-0728(84)80324-1

Ciampi, S., and Di castro, V. (1995). XPS Study of the Growth and Reactivity of FeMnO Thin Films. *Surf. Sci.* 331, 294–299. doi:10.1016/0039-6028(95)00190-5

Cuán, A., Galván, M., and Chattaraj, P. K. (2005). A Philicity Based Analysis of Adsorption of Small Molecules in Zeolites. *J. Chem. Sci.* 117, 541–548. doi:10.1007/BF02708360

Domingo, L., Ríos-Gutiérrez, M., and Pérez, P. (2016). Applications of the Conceptual Density Functional Theory Indices to Organic Chemistry Reactivity. *Molecules* 21, 748. doi:10.3390/molecules21060748

Ech-chihbi, E., Belghiti, M. E., Salim, R., Oudda, H., Taleb, M., Benchat, N., et al. (2017). Experimental and Computational Studies on the Inhibition Performance of the Organic Compound "2-phenylimidazo [1,2-A] pyrimidine-3-Carbaldehyde" against the Corrosion of Carbon Steel in 1.0 M HCl Solution. *Surf. Inter.* 9, 206–217. doi:10.1016/j.surfin.2017.09.012

Ehteshamzade, M., Shahrabi, T., and Hosseini, M. G. (2006). Inhibition of Copper Corrosion by Self-Assembled Films of New Schiff Bases and Their Modification with Alkanethiols in Aqueous Medium. *Appl. Surf. Sci.* 252, 2949–2959. doi:10.1016/j.apsusc.2005.05.003

El Azzouzi, M., Aouniti, A., Tighadouin, S., Elmsellem, H., Radi, S., Hammouti, B., et al. (2016). Some Hydrazine Derivatives as Corrosion Inhibitors for Mild Steel in 1.0M HCl: Weight Loss, Electrochemichal, SEM and Theoretical Studies. *J. Mol. Liquids* 221, 633–641. doi:10.1016/j.molliq.2016.06.007

El Faydy, M., Benhiba, F., Lakhrissi, B., Touhami, M. E., Warad, I., Bentiss, F., et al. (2019). The Inhibitive Impact of Both Kinds of 5-Isothiocyanatomethyl-8-Hydroxyquinoline Derivatives on the Corrosion of Carbon Steel in Acidic Electrolyte. *J. Mol. Liquids* 295, 111629. doi:10.1016/j.molliq.2019.111629

El Faydy, M., Touir, R., Ebn Touhami, M., Zarrouk, A., Jama, C., Lakhrissi, B., et al. (2018). Corrosion Inhibition Performance of Newly Synthesized 5-Alkoxymethyl-8-Hydroxyquinoline Derivatives for Carbon Steel in 1 M HCl Solution: Experimental, DFT and Monte Carlo Simulation Studies. *Phys. Chem. Chem. Phys.* 20, 20167–20187. doi:10.1039/C8CP03226B

El-Hajjaji, F., Messali, M., Aljuhani, A., Aouad, M. R., Hammouti, B., Belghiti, M. E., et al. (2018). Pyridazinium-based Ionic Liquids as Novel and green Corrosion Inhibitors of Carbon Steel in Acid Medium: Electrochemical and Molecular Dynamics Simulation Studies. *J. Mol. Liquids* 249, 997–1008. doi:10.1016/j.molliq.2017.11.111

El-Hajjaji, F., Messali, M., Martínez de Yuso, M. V., Rodríguez-Castellón, E., Almutairi, S., Bandosz, T. J., et al. (2019). Effect of 1-(3-phenoxypropyl) Pyridazin-1-Ium Bromide on Steel Corrosion Inhibition in Acidic Medium. *J. Colloid Interf. Sci.* 541, 418–424. doi:10.1016/j.jcis.2019.01.113

El-Taib Heakal, F., Tantawy, N. S., and Shehata, O. S. (2012). Influence of Cerium (III) Ions on Corrosion and Hydrogen Evolution of Carbon Steel in Acid Solutions. *Int. J. Hydrogen Energ.* 37, 19219–19230. doi:10.1016/j.ijhydene.2012.10.037

Fan, C., Zhang, B., Li, Y., Liang, Y., Xue, X., and Feng, Y. (2015). Application-oriented Computational Studies on a Series of D-π-A Structured Porphyrin Sensitizers with Different Electron-Donor Groups. *Phys. Chem. Chem. Phys.* 17, 30624–30631. doi:10.1039/C5CP05625J

Farhadian, A., Varfolomeev, M. A., Rahimi, A., Mendgaziev, R. I., Semenov, A. P., Stoporev, A. S., et al. (2021). Gas Hydrate and Corrosion Inhibition Performance of the Newly Synthesized Polyurethanes: Potential Dual Function Inhibitors. *Energy Fuels* 35, 6113–6124. doi:10.1021/acs.energyfuels.1c00101

Finšgar, M., Fassbender, S., Hirth, S., and Milošev, I. (2009). Electrochemical and XPS Study of Polyethyleneimines of Different Molecular Sizes as Corrosion Inhibitors for AISI 430 Stainless Steel in Near-Neutral Chloride media. *Mater. Chem. Phys.* 116, 198–206. doi:10.1016/j.matchemphys.2009.03.010

Geerlings, P., Ayers, P. W., Toro-Labbé, A., Chattaraj, P. K., and De Proft, F. (2012). The Woodward-Hoffmann Rules Reinterpreted by Conceptual Density Functional Theory. *Acc. Chem. Res.* 45, 683–695. doi:10.1021/ar200192t

Gomma, G. K., and Wahdan, M. H. (1995). Schiff Bases as Corrosion Inhibitors for Aluminium in Hydrochloric Acid Solution. *Mater. Chem. Phys.* 39, 209–213. doi:10.1016/0254-0584(94)01436-K

Guo, L., Kaya, S., Obot, I. B., Zheng, X., and Qiang, Y. (2017). Toward Understanding the Anticorrosive Mechanism of Some Thiourea Derivatives for Carbon Steel Corrosion: a Combined DFT and Molecular Dynamics Investigation. *J. Colloid Interf. Sci.* 506, 478–485. doi:10.1016/j.jcis.2017.07.082

Haque, J., Srivastava, V., Verma, C., and Quraishi, M. A. (2017). Experimental and Quantum Chemical Analysis of 2-amino-3-((4-((S)-2-Amino-2-Carboxyethyl)-1h-Imidazol-2-Yl)thio) Propionic Acid as New and green Corrosion Inhibitor for Mild Steel in 1 M Hydrochloric Acid Solution. *J. Mol. Liquids* 225, 848–855. doi:10.1016/j.molliq.2016.11.011

Hsissou, R., Benhiba, F., Dagdag, O., El Bouchti, M., Nouneh, K., Assouag, M., et al. (2020). Development and Potential Performance of Prepolymer in Corrosion Inhibition for Carbon Steel in 1.0 M HCl: Outlooks from Experimental and Computational Investigations. *J. Colloid Interf. Sci.* 574, 43–60. doi:10.1016/j.jcis.2020.04.022

Kannan, P., Jithinraj, P., and Natesan, M. (2014). Multiphasic Inhibition of Mild Steel Corrosion in H2S Gas Environment. *Arab. J. Chem.* 11, 388–404. doi:10.1016/j.arabjc.2014.10.032

Khadiri, A., Ousslim, A., Bekkouche, K., Aouniti, A., Warad, I., Elidrissi, A., et al. (2018). 4-(2-(2-(2-(2-(Pyridine-4-yl)ethylthio)ethoxy)ethylthio)ethyl)pyridine as New Corrosion Inhibitor for Mild Steel in 1.0 M HCl Solution: Experimental and Theoretical Studies. *J. Bio. Tribo Corros.* 4, 64. doi:10.1007/s40735-018-0179-3

Khadraoui, A., Khelifa, A., Hadjmeliani, M., Mehdaoui, R., Hachama, K., Tidu, A., et al. (2016). Extraction, Characterization and Anti-corrosion Activity of Mentha Pulegium Oil: Weight Loss, Electrochemical, Thermodynamic and Surface Studies. *J. Mol. Liquids* 216, 724–731. doi:10.1016/j.molliq.2016.02.005

Khaled, K. F. (2010). Experimental, Density Function Theory Calculations and Molecular Dynamics Simulations to Investigate the Adsorption of Some Thiourea Derivatives on Iron Surface in Nitric Acid Solutions. *Appl. Surf. Sci.* 256, 6753–6763. doi:10.1016/j.apsusc.2010.04.085

Kozlica, D. K., Kokalj, A., and Milošev, I. (2021). Synergistic Effect of 2-mercaptobenzimidazole and Octylphosphonic Acid as Corrosion Inhibitors for Copper and Aluminium - an Electrochemical, XPS, FTIR and DFT Study. *Corrosion Sci.* 182, 109082. doi:10.1016/j.corsci.2020.109082

Laabaissi, T., Benhiba, F., Rouifi, Z., Missioui, M., Ourrak, K., Oudda, H., et al. (2019). New Quinoxaline Derivative as a green Corrosion Inhibitor for Mild Steel in Mild Acidic Medium: Electrochemical and Theoretical Studies. *Int. J. Corros. Scale Inhib.* 8, 241–256. doi:10.17675/2305-6894-2019-8-2-6

Lee, C., Yang, W., and Parr, R. G. (1988). Local Softness and Chemical Reactivity in the Molecules CO, SCN− and H2CO. *J. Mol. Struct. THEOCHEM* 163, 305–313. doi:10.1016/0166-1280(88)80397-X

Li, H., Zhang, S., and Qiang, Y. (2021). Corrosion Retardation Effect of a green Cauliflower Extract on Copper in H2SO4 Solution: Electrochemical and Theoretical Explorations. *J. Mol. Liquids* 321, 114450. doi:10.1016/j.molliq.2020.114450

Lukovits, I., Kálmán, E., and Zucchi, F. (2001). Corrosion Inhibitors-Correlation between Electronic Structure and Efficiency. *Corrosion* 57, 3–8. doi:10.5006/1.3290328

McCafferty, E., and Hackerman, N. (1972). Double Layer Capacitance of Iron and Corrosion Inhibition with Polymethylene Diamines. *J. Electrochem. Soc.* 119, 146–154. doi:10.1149/1.2404150

Meeusen, M., Zardet, L., Homborg, A. M., Lekka, M., Andreatta, F., Fedrizzi, L., et al. (2020). The Effect of Time Evolution and Timing of the Electrochemical Data Recording of Corrosion Inhibitor protection of Hot-Dip Galvanized Steel. *Corrosion Sci.* 173, 108780. doi:10.1016/j.corsci.2020.108780

Mishra, A., Aslam, J., Verma, C., Quraishi, M. A., and Ebenso, E. E. (2020). Imidazoles as Highly Effective Heterocyclic Corrosion Inhibitors for Metals and Alloys in Aqueous Electrolytes: A Review. *J. Taiwan Inst. Chem. Eng.* 114, 341–358. doi:10.1016/j.jtice.2020.08.034

Monticelli, C., Balbo, A., Esvan, J., Chiavari, C., Martini, C., Zanotto, F., et al. (2019). Evaluation of 2-(salicylideneimino) Thiophenol and Other Schiff Bases as Bronze Corrosion Inhibitors by Electrochemical Techniques and Surface Analysis. *Corrosion Sci.* 148, 144–158. doi:10.1016/j.corsci.2018.12.017

Morell, C., Grand, A., and Toro-Labbé, A. (2006). Theoretical Support for Using the Δf(r) Descriptor. *Chem. Phys. Lett.* 425, 342–346. doi:10.1016/j.cplett.2006.05.003

Nahle, A., El-Hajjaji, F., Ghazoui, A., Benchat, N.-E., Taleb, M., Saddik, R., et al. (2018). Effect of Substituted Methyl Group by Phenyl Group in Pyridazine Ring on the Corrosion Inhibition of Mild Steel in 1.0 M HCl. *Acmm* 65, 87–96. doi:10.1108/acmm-03-2017-1769

Ouici, H., Tourabi, M., Benali, O., Selles, C., Jama, C., Zarrouk, A., et al. (2017). Adsorption and Corrosion Inhibition Properties of 5-amino 1,3,4-Thiadiazole-2-Thiol on the Mild Steel in Hydrochloric Acid Medium: Thermodynamic, Surface and Electrochemical Studies. *J. Electroanalytical Chem.* 803, 125–134. doi:10.1016/j.jelechem.2017.09.018

Padmanabhan, J., Parthasarathi, R., Subramanian, V., and Chattaraj, P. K. (2006). Chemical Reactivity Indices for the Complete Series of Chlorinated Benzenes: Solvent Effect. *J. Phys. Chem. A.* 110, 2739–2745. doi:10.1021/jp056630a

Pan, C., Song, Y., Jin, W., Qin, Z., Song, S., Hu, W., et al. (2020). Enhancing the Stability of Passive Film on 304 SS by Chemical Modification in Alkaline Phosphate-Molybdate Solutions. *Trans. Tianjin Univ.* 26, 135–141. doi:10.1007/s12209-020-00238-8

Parr, R. G., and Yang, W. (1984). Density Functional Approach to the Frontier-Electron Theory of Chemical Reactivity. *J. Am. Chem. Soc.* 106, 4049–4050. doi:10.1021/ja00326a036

Parthasarathi, R., Padmanabhan, J., Elango, M., Subramanian, V., and Chattaraj, P. K. (2004). Intermolecular Reactivity through the Generalized Philicity Concept. *Chem. Phys. Lett.* 394, 225–230. doi:10.1016/j.cplett.2004.07.002

Pech-Canul, M. A., and Bartolo-Pérez, P. (2004). Inhibition Effects of N-phosphono-methyl-glycine/Zn2+ Mixtures on Corrosion of Steel in Neutral Chloride Solutions. *Surf. Coat. Techn.* 184, 133–140. doi:10.1016/j.surfcoat.2003.11.018

Qiang, Y., Guo, L., Li, H., and Lan, X. (2021). Fabrication of Environmentally Friendly Losartan Potassium Film for Corrosion Inhibition of Mild Steel in HCl Medium. *Chem. Eng. J.* 406, 126863. doi:10.1016/j.cej.2020.126863

Qiang, Y., Li, H., and Lan, X. (2020). Self-assembling Anchored Film Basing on Two Tetrazole Derivatives for Application to Protect Copper in Sulfuric Acid Environment. *J. Mater. Sci. Techn.* 52, 63–71. doi:10.1016/j.jmst.2020.04.005

Qiang, Y., Zhang, S., Guo, L., Zheng, X., Xiang, B., and Chen, S. (2017). Experimental and Theoretical Studies of Four Allyl Imidazolium-Based Ionic Liquids as green Inhibitors for Copper Corrosion in Sulfuric Acid. *Corrosion Sci.* 119, 68–78. doi:10.1016/j.corsci.2017.02.021

Qiang, Y., Zhang, S., Tan, B., and Chen, S. (2018). Evaluation of Ginkgo Leaf Extract as an Eco-Friendly Corrosion Inhibitor of X70 Steel in HCl Solution. *Corrosion Sci.* 133, 6–16. doi:10.1016/j.corsci.2018.01.008

Raevsky, O. A., Grigor'ev, V. Y., Liplavskaya, E. A., and Worth, A. P. (2011). Prediction of Acute Rodent Toxicity on the Basis of Chemical Structure and Physicochemical Similarity. *Mol. Inf.* 30, 267–275. doi:10.1002/minf.201000145

Rahmani, H., Alaoui, K. I., Azzouzi, M. E., Benhiba, F., Hallaoui, A. E., Rais, Z., et al. (2019a). Corrosion Assessement of Mild Steel in Acid Environment Using Novel Triazole Derivative as a Anti-corrosion Agent: A Combined Experimental and Quantum Chemical Study. *Chem. Data Collections* 24, 100302. doi:10.1016/j.cdc.2019.100302

Rahmani, H., Alaoui, K. I., Emran, K. M., El Hallaoui, A., Taleb, M., El Hajji, S., et al. (2019b). Experimental and DFT Investigation on the Corrosion Inhibition of Mild Steel by 1, 2, 3- Triazole Regioisomers in 1M Hydrochloric Acid Solution. *Int. J. Electrochem. Sci.* 14, 985–998. doi:10.20964/2019.01.80

Rbaa, M., Benhiba, F., Obot, I. B., Oudda, H., Warad, I., Lakhrissi, B., et al. (2019). Two New 8-hydroxyquinoline Derivatives as an Efficient Corrosion Inhibitors for Mild Steel in Hydrochloric Acid: Synthesis, Electrochemical, Surface Morphological, UV-Visible and Theoretical Studies. *J. Mol. Liquids* 276, 120–133. doi:10.1016/j.molliq.2018.11.104

Saady, A., Rais, Z., Benhiba, F., Salim, R., Ismaily Alaoui, K., Arrousse, N., et al. (2021). Chemical, Electrochemical, Quantum, and Surface Analysis Evaluation on the Inhibition Performance of Novel Imidazo[4,5-B] Pyridine Derivatives against Mild Steel Corrosion. *Corrosion Sci.* 189, 109621. doi:10.1016/j.corsci.2021.109621

Salhi, A., Tighadouini, S., El-Massaoudi, M., Elbelghiti, M., Bouyanzer, A., Radi, S., et al. (2017). Keto-enol Heterocycles as New Compounds of Corrosion

Inhibitors for Carbon Steel in 1 M HCl: Weight Loss, Electrochemical and Quantum Chemical Investigation. *J. Mol. Liquids* 248, 340–349. doi:10.1016/j.molliq.2017.10.040

Salim, R., Ech-chihbi, E., Oudda, H., El Hajjaji, F., Taleb, M., and Jodeh, S. (2019). A Review on the Assessment of Imidazo[1,2-A]pyridines as Corrosion Inhibitor of Metals. *J. Bio. Tribo Corros.* 5, 14. doi:10.1007/s40735-018-0207-3

Singh, A. K., and Quraishi, M. A. (2010). Effect of Cefazolin on the Corrosion of Mild Steel in HCl Solution. *Corrosion Sci.* 52, 152–160. doi:10.1016/j.corsci.2009.08.050

Singh, D. K., Kumar, S., Udayabhanu, G., and John, R. P. (2016). 4(N,N-dimethylamino) Benzaldehyde Nicotinic Hydrazone as Corrosion Inhibitor for Mild Steel in 1 M HCl Solution: An Experimental and Theoretical Study. *J. Mol. Liquids* 216, 738–746. doi:10.1016/j.molliq.2016.02.012

Sliem, M. H., Afifi, M., Bahgat Radwan, A., Fayyad, E. M., Shibl, M. F., Heakal, F. E.-T., et al. (2019). AEO7 Surfactant as an Eco-Friendly Corrosion Inhibitor for Carbon Steel in HCl Solution. *Sci. Rep.* 9, 2319. doi:10.1038/s41598-018-37254-7

Sun, H. (1998). COMPASS: An Ab Initio Force-Field Optimized for Condensed-phase ApplicationsOverview with Details on Alkane and Benzene Compounds. *J. Phys. Chem. B* 102, 7338–7364. doi:10.1021/jp980939v

Tang, Y., Zhang, F., Hu, S., Cao, Z., Wu, Z., and Jing, W. (2013). Novel Benzimidazole Derivatives as Corrosion Inhibitors of Mild Steel in the Acidic media. Part I: Gravimetric, Electrochemical, SEM and XPS Studies. *Corrosion Sci.* 74, 271–282. doi:10.1016/j.corsci.2013.04.053

Temesghen, W., and Sherwood, P. (2002). Analytical Utility of Valence Band X-ray Photoelectron Spectroscopy of Iron and its Oxides, with Spectral Interpretation by Cluster and Band Structure Calculations. *Anal. Bioanal. Chem.* 373, 601–608. doi:10.1007/s00216-002-1362-3

Wagner, C. D., Riggs, W. M., Davis, L. E., Moulder, J. F., and Muilenberg, G. E. (1979). *Handbook of X-Ray Photoelectron Spectroscopy*. USA: Perking-Elmer Corporation, Physical Electronics Division.

Watts, J. F., and Wolstenholme, J. (2003). *An Introduction to Surface Analysis by XPS and AES*. UK: John Wiley & Sons.

Weng, L. T., Poleunis, C., Bertrand, P., Carlier, V., Sclavons, M., Franquinet, P., et al. (1995). Sizing Removal and Functionalization of the Carbon Fiber Surface Studied by Combined TOF SIMS and XPS. *J. Adhes. Sci. Techn.* 9, 859–871. doi:10.1163/156856195X00743

Xia, D.-H., Pan, C., Qin, Z., Fan, B., Song, S., Jin, W., et al. (2020). Covalent Surface Modification of LY12 Aluminum alloy Surface by Self-Assembly Dodecyl Phosphate Film towards Corrosion protection. *Prog. Org. Coat.* 143, 105638. doi:10.1016/j.porgcoat.2020.105638

Yamashita, T., and Hayes, P. (2008). Analysis of XPS Spectra of Fe2+ and Fe3+ Ions in Oxide Materials. *Appl. Surf. Sci.* 254, 2441–2449. doi:10.1016/j.apsusc.2007.09.063

Zarrouk, A., Zarrok, H., Ramli, Y., Bouachrine, M., Hammouti, B., Sahibed-dine, A., et al. (2016). Inhibitive Properties, Adsorption and Theoretical Study of 3,7-Dimethyl-1-(prop-2-Yn-1-Yl)quinoxalin-2(1h)-One as Efficient Corrosion Inhibitor for Carbon Steel in Hydrochloric Acid Solution. *J. Mol. Liquids* 222, 239–252. doi:10.1016/j.molliq.2016.07.046

Zhang, F., Tang, Y., Cao, Z., Jing, W., Wu, Z., and Chen, Y. (2012). Performance and Theoretical Study on Corrosion Inhibition of 2-(4-Pyridyl)-Benzimidazole for Mild Steel in Hydrochloric Acid. *Corrosion Sci.* 61, 1–9. doi:10.1016/j.corsci.2012.03.045

Zhang, G. A., Hou, X. M., Hou, B. S., and Liu, H. F. (2019a). Benzimidazole Derivatives as Novel Inhibitors for the Corrosion of Mild Steel in Acidic Solution: Experimental and Theoretical Studies. *J. Mol. Liquids* 278, 413–427. doi:10.1016/j.molliq.2019.01.060

Zhang, Q. H., Hou, B. S., Li, Y. Y., Zhu, G. Y., Lei, Y., Wang, X., et al. (2021). Dextran Derivatives as Highly Efficient green Corrosion Inhibitors for Carbon Steel in CO2-saturated Oilfield Produced Water: Experimental and Theoretical Approaches. *Chem. Eng. J.* 424, 130519. doi:10.1016/j.cej.2021.130519

Zhang, S. D., Wu, J., Qi, W. B., and Wang, J. Q. (2016). Effect of Porosity Defects on the Long-Term Corrosion Behaviour of Fe-Based Amorphous alloy Coated Mild Steel. *Corrosion Sci.* 110, 57–70. doi:10.1016/j.corsci.2016.04.021

Zhang, W., Li, H.-J., Wang, M., Wang, L.-J., Pan, Q., Ji, X., et al. (2019b). Tetrahydroacridines as Corrosion Inhibitor for X80 Steel Corrosion in Simulated Acidic Oilfield Water. *J. Mol. Liquids* 293, 111478. doi:10.1016/j.molliq.2019.111478

Zhao, H., Zhang, X., Ji, L., Hu, H., and Li, Q. (2014). Quantitative Structure-Activity Relationship Model for Amino Acids as Corrosion Inhibitors Based on the Support Vector Machine and Molecular Design. *Corrosion Sci.* 83, 261–271. doi:10.1016/j.corsci.2014.02.023

Zhao, Z., Sun, J., Tang, H., and Yan, X. (2020). Experimental and Theoretical Studies of Cinnamyl Alcohol as a Novel Corrosion Inhibitor for Copper Foils in Rolling Oil. *Mater. Corrosion* 72, 534–542. doi:10.1002/maco.202011887

Conflict of Interest: The authors declare that the research was conducted in the absence of any commercial or financial relationships that could be construed as a potential conflict of interest.

Publisher's Note: All claims expressed in this article are solely those of the authors and do not necessarily represent those of their affiliated organizations or those of the publisher, the editors and the reviewers. Any product that may be evaluated in this article, or claim that may be made by its manufacturer, is not guaranteed or endorsed by the publisher.